Mesoporous Silica Nanoparticles: Selective Surface Functionalization for Optimal Relaxometric and Drug Loading Performances

Meryem Bouchoucha, René C.-Gaudreault, Marc-André Fortin, and Freddy Kleitz**

Mesoporous silica nanoparticles (MSNs) have emerged as promising biomaterials for drug delivery and cell tracking applications, for which MRI is the medical imaging modality of choice. In this contribution, MRI contrast agents (DTPA-Gd) and polyethylene glycol (PEG) are grafted selectively at the surface of MSNs, in order to achieve optimal relaxometric and drug loading performances. In fact, DTPA and PEG grafting procedures reported until now, have resulted in significant pore obstruction, which is detrimental to the drug delivery function of MSNs. This usually induces a dramatic decrease in surface area and pore volume, thus limiting drug loading capacity. Therefore, these molecules must be selectively grafted at the outer surface of MSNs. In this study, 3D pore network MSNs (MCM-48-type) are synthesized and functionalized with a straightforward and efficient grafting procedure in which DTPA and PEG are selectively grafted at the outer surface of MSNs. No pore blocking is observed, and more than 90% of surface area, pore volume and pore diameter are retained. The thus-treated particles are colloidally stable in SBF and cell culture media, they are not cytotoxic and they have high drug loading capacity. Upon labeling with Gd, the nanoparticle suspensions have strong relaxometric properties ($r_2/r_1 = 1.47$, $r_1 = 23.97\ mM^{-1}\ s^{-1}$), which confers a remarkable positive contrast enhancement potential to the compound. The particles could serve as efficient drug carriers, as demonstrated with a model of daunorubicin submitted to physiological conditions. The selective nanoparticle surface grafting procedures described in the present article represent a significant advance in the design of high colloidal stability silica-based vectors with high drug loading capacity, which could provide novel theranostic nanocompounds.

1. Introduction

Mesoporous silica nanoparticles (MSNs) have emerged as promising materials for drug delivery.[1] The size, structure, and chemistry of these biocompatible materials can be precisely controlled.[1i,2] MSNs have been explored as potential drug delivery systems for a variety of therapeutic agents[1j,3] (e.g., anti-cancer molecules).[4] In the field of chemotherapy, MSNs have been proven to strongly accumulate in tumors by passive targeting via the enhanced permeability and retention effect[4d,5] or by active targeting via grafting of specific cancer cell-targeting molecules.[6] Furthermore, mesoporous silica and core-shell silica-based nanoparticles are now entering clinical trials as therapeutic/diagnostic compounds.[7]

Recently, research efforts on MSNs for drug delivery have focused on the development of theranostic nanoparticles which combine simultaneous therapeutic and imaging capabilities.[8] Imaging the distribution of drug delivery vectors (in blood and in organs) in the minutes following injection, would allow recording more precise and more personalized pharmacokinetics and drug delivery data (i.e., overall biodistribution, organ delivery

Prof. F. Kleitz, M. Bouchoucha
Department of Chemistry
Université Laval
Québec QC, G1V 0A6, Canada
E-mail: freddy.kleitz@chm.ulaval.ca
Prof. R. C.-Gaudreault
Centre de recherche du Centre hospitalier
universitaire de Québec (CR-CHUQ)
axe Cancer
QC,Québec G1L 3L5, Canada
Prof. R. C.-Gaudreault
Department of Molecular Medicine
Université Laval
Québec, QC G1V 0A6, Canada
DOI: 10.1002/adfm.201400524

Prof. M.-A. Fortin, M. Bouchoucha
Centre de recherche du Centre hospitalier
universitaire de Québec (CR-CHUQ)
axe Médecine Régénératrice,
QC Québec, G1L 3L5, Canada
E-mail: marc-andre.fortin@gmn.ulaval.ca
Prof. M.-A. Fortin, M. Bouchoucha
Department of Mining, Metallurgy
and Materials Engineering
Université Laval
QC Québec, G1V 0A6, Canada
Prof. F. Kleitz, Prof. M.-A. Fortin, M. Bouchoucha
Centre de recherche sur les matériaux avancés (CERMA)
Université Laval
Québec, G1V 0A6, Canada

effectiveness, targeting efficiency). Among imaging modalities, MRI enables whole-body imaging without the use of ionizing radiation.[9] This non-invasive diagnostic tool, which is based on the excitation of ^{1}H protons in hydrated tissues, is widely used in pre-clinical research as well as in clinical procedures (e.g., in oncology).[10]

Among all structural characteristics of MSNs that make them versatile as drug vectors, the most important are their high surface area and high pore volume. These characteristics allow the uptake of large amounts of therapeutic molecules. Nevertheless, in order to design optimal theranostic MSNs that bear a dual capacity as drug delivery vehicles and imaging probes, these nanoparticles must achieve the following three (3) criteria: 1) biocompatible (macro)molecules used to enhance colloidal stability and blood retention must be selectively grafted on the external surface of the particles; 2) biomedical imaging functional groups must be efficiently grafted at the surface of the pores, and 3) the grafting of all these molecules should not result in a drastic decrease of the nanoparticle porosity, which is necessary to preserve the drug delivery functionality of the MSNs nanocarriers.

Polyethylene glycol (PEG) grafted at the outer surface of MSNs, improves their colloidal stability under physiological conditions, as well as bio- and hemocompatibility. It helps conditioning MSNs for intravenous injections.[11] PEGylation usually increases blood circulation half-life time, and allows higher accumulation of nanoparticles at tumor sites.[5b,12] However, almost invariably, the PEG grafting procedures that were developed thus far have resulted in significant pore obstruction (surface area and pore volume loss between 32 and 70%), which is detrimental to the drug delivery function of MSNs.[11a,12d,13] One important aspect of this problem relates to the fact that PEG are mobile linear chains that can diffuse slowly into the mesopores and, ultimately, fill the pore volume.

Imaging probes, which are grafted either at the outer surface or at the mesopore surface of MSNs, allow their tracking *in vivo*. In particular, labeling MSNs with Gd-based MRI contrast agents, results in high-relaxivity imaging probes that are easily tracked in the blood as well as in key organs such as liver and spleen, where they are expected to accumulate.[14]

Gd(III) chelates (e.g., DTPA, diethylenetriaminopentaacetic acid) attached to the surface of nanoparticles, are used as "positive" contrast agents, i.e. their presence at certain concentrations induces MR signal brightening.[15] However, chelate grafting at the surface of MSNs further affects their final pore volume, and represents another important factor leading to MSNs pore obstruction. For conventional MSNs with an average pore diameter initially included between 2–4 nm, chelate grafting results in pore diameter decrease in the order of 24 to 63% [14c,16] with pore volume and surface area loss of 30 – 52%.[16,17] Although several studies have reported Gd-labeled MSNs (e.g., Gd-chelates-MSNs), none of these have demonstrated the possibility to label MSNs with MRI contrast agents, while preserving their drug-loading and elution ability. Indeed, the best case reported featured the retention of only 56% of surface area and pore volume after grafting of both DTPA-Gd and PEG.[14d] PEGylation and co-grafting of metal chelates inevitably affect the availability of drug adsorption sites, and therefore the drug loading capacity of MSNs. This appears to be one of the main factors limiting the development of MSNs for drug delivery applications. Thus, preserving the porosity of the nanoparticles (e.g., surface area and pore volume) is of central interest in the current research on MSNs for drug elution applications.

While PEGylation confers enhanced colloidal stability, and Gd-DTPA the MRI enhancement functionality, the drug elution capacity of surface-grafted MSNs must also be demonstrated. *In vivo*, the drugs contained by MSNs must be efficiently and selectively released at specific sites (a tumor, or a specific organ). For this purpose, different controlled drug release strategies have been developed until now, based on various stimuli: pH,[4c,e,i,18] enzyme actions,[19] redox reaction,[20] photoirradiation,[19a,21] to mention a few. Among these, pH-responsive mechanisms are particularly interesting and widely investigated. For instance, the pH of extracellular fluid in tumor environment (pH 6.2) is more acidic than in healthy tissues (pH 7.4).[22] Moreover, when MSNs are internalized within cells, they are most often entrapped in endosomes and lysosomes. The pH of these cellular compartments (pH = 4.5–5.5) is lower than that of normal cells (pH ≈ 6).[23] Thus, this pH transition could also be strategically exploited.[24] Different mechanisms have been proposed to confer a pH-delivery functionality to MSNs, based on the grafting of organic functional groups[4c] into the MSNs pores, as well as polymers,[25] proteins[18g] and supramolecular molecules[26] on their outer surface. Besides, an efficient pH-responsive mechanism can simply be based on protonation/deprotonation of the silanol groups (–SiOH) located at the surface of porous silica frameworks. This latter strategy was pursued here to enable the uptake and release of daunorubicin.

In the present study, MSNs were designed as potential theranostic nanocarriers with the ability to provide: 1) high drug loading capacity (the highest pore volume achieved thus far for PEG and Gd-chelate-grafted MSNs); 2) the most efficient MRI positive contrast enhancement potential reported thus far for mesoporous silica nanoparticles; 3) high drug loading and controlled drug release in physiological media. In fact, the design of optimal drug delivery vehicles is simply not possible if pores are filled-up with PEG, chelates, as well as other surfactants. The present study is the first demonstration of the preservation of significant pore volumes after grafting of PEG and Gd-chelates on MSNs. To achieve this goal, MCM-48-type MSNs were synthesized and co-reacted with DTPA-silane and PEG-silane molecules. The optimal amount of these molecules, necessary to cover only the outer surface of MSNs, was precisely determined. This specific strategy generates a truly selective grafting of the outer surface without pore obstruction and porosity loss. After chelation with Gd^{3+}, the relaxometric performance of these nanoparticles was measured and demonstrated *in vitro* with T_1-weighted imaging MR sequences. The colloidal stability and *in vitro* biocompatibility of these nanoparticles was also investigated. Finally, the capacity of these functionalized nanoparticles to trap drug molecules and to control their release was evaluated in PBS (pH 7.4) and in acetate buffer solution (pH 5 and 4).

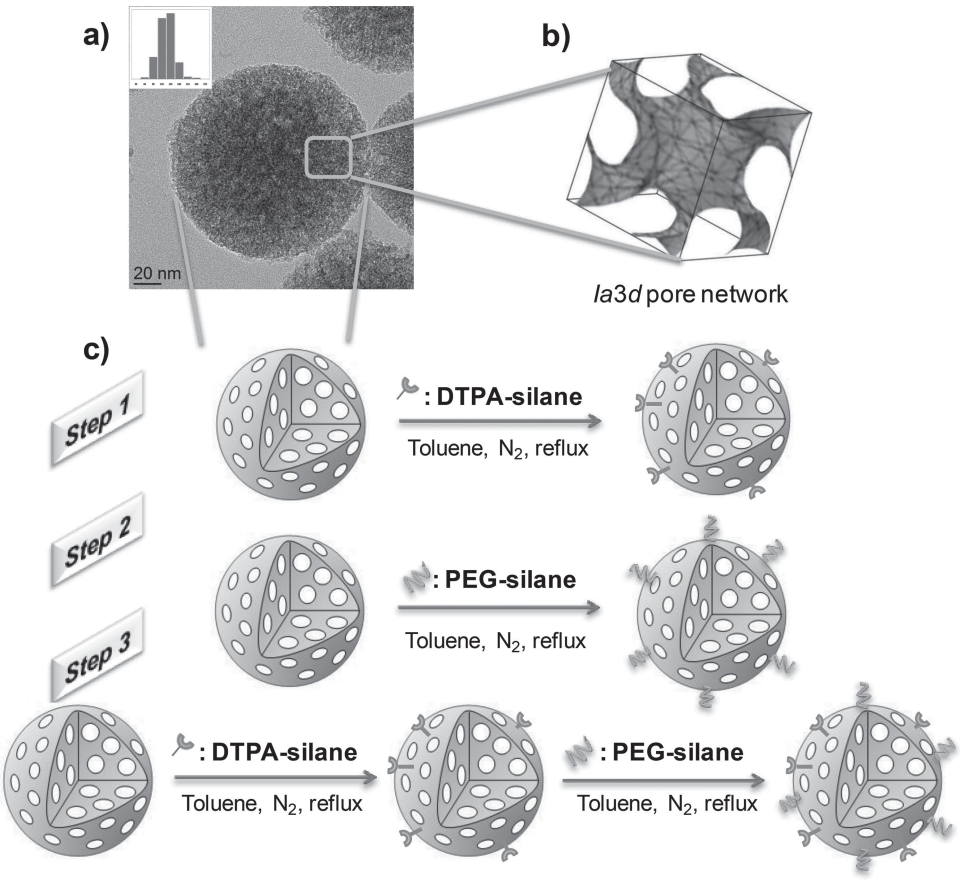

Figure 1. a) MCM-48 nanoparticles imaged by TEM; b) Schematic representation in the *Ia3d* 3-D cubic pore network in the MCM-48 particles; c) Schematic representation of the three steps undertaken to optimize PEG and DTPA grafting.

2. Results and Discussion

2.1. Synthesis and Physicochemical Characterization

Pristine MCM-48-type mesoporous silica nanoparticles were synthesized according to a previously reported procedure.[27] Transmission electron microscopy (TEM) observations revealed well-defined spherical particles with an average particle diameter of 150 nm (**Figure 1**-a-b). Low-angle XRD data showed typical peaks of highly ordered 3-D cubic *Ia3d* mesopore structure (Figure S1-a, Supporting Information). MCM-48 nanoparticles showed type IV N_2 physisorption isotherms characteristic of uniform mesoporous channels with narrow, cylindrical pores (Figure S1-b, Supporting Information). These nanoparticles showed a high specific surface area (1654 $m^2.g^{-1}$; BET method), and a large total pore volume (0.82 $cm^3\ g^{-1}$). The mean pore diameter was estimated at 3 nm (NLDFT method, Figure S1-c, Supporting Information).

The grafting optimization of DTPA and PEG on MSNs was achieved in three steps (Figure 1-c). First (step 1), by carefully controlling DTPA grafting; then (step 2), by tuning the amount of PEG used for grafting. For this, large PEG-silane molecules (20 kDa) were used. The hydrodynamic diameter of 20 kDa PEG is about 9 nm in PBS 10 mM pH 7.4,[28] which is well above the diameter of the MSN pores (~3 nm), in contrast to the more usual PEG molecules of smaller molecular weight (2.6 nm diameter for 2 kD PEG). Therefore, such large molecules (20 kDa) are not expected to crawl efficiently into the pores of the 150-nm diameter MSNs, and will most likely remain at the exterior of the MSN structure. At high concentrations, a small but effective fraction of PEG-silane could be attached on the apertures of the pores, thereby causing pore obstruction and a subsequent loss of accessible total pore volume. For this reason, it is absolutely important to reach well-balanced DTPA and PEG grafting conditions. Finally (step 3), DTPA and PEG were successfully used to demonstrate the possibility of grafting preferentially at the outer surface of MSNs, both the metal chelates and the biocompatible molecules providing steric hindrance to the MCM-48 system. The resulting nanoparticles are designated by "MSN-*x*DTPA-*y*PEG", where *x* corresponds to the percentage of grafted DTPA-silane and *y* to the percentage of grafted PEG-silane. In particular, the optimization of DTPA grafting (step 1 – Figure 1-c) was carried out by adding different amounts of DTPA-silane (DTPA-silane: DTPA+APTES). According to the thermogravimetric analysis (TGA) results, the percentage of grafted DTPA-silane (w/w), was varied between 3 and 13% depending of the reaction conditions used (Figure S2-a, Supporting Information). The resulting nanoparticles are designated by "MSN-*x*DTPA". The PEG grafting optimization (step 2 – Figure 1-c) was also carried out

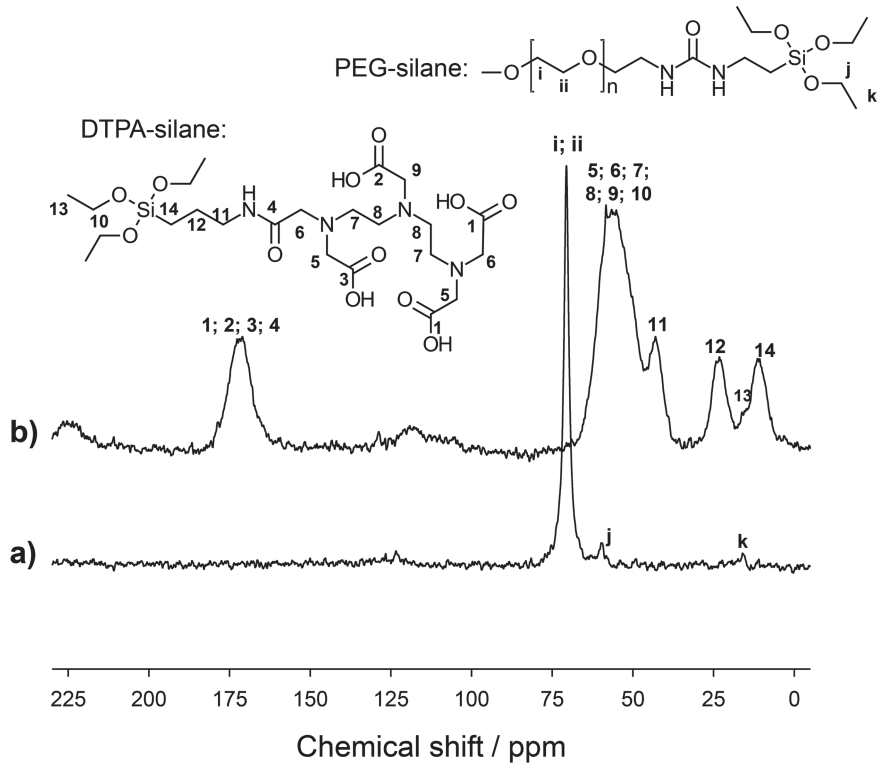

Assignment	δ [ppm]
C(1); C(2); C(3); C(4): C=O in COOH and CONH	172 - 176
C(5); C(6); C(7); C(8); C(9); C(10): CH_2-N and CH_2-O	58.3 – 54.9
C(11); C(12); C(13); C(14)	43.2; 23.9; 15.5; 11.2

Figure 2. ^{13}C CP MAS NMR spectra of: a) MSN-*x*PEG and b) MSN-*y*DTPA; *x* = 10.5% and *y* = 9%; similar peaks were found for the different combinations of DTPA and PEG concentrations investigated.

by adding different amounts of PEG-silane (20 kDa). The percentage of grafted PEG-silane (w/w), estimated by TGA, ranged between 3.5 and 27% (Figure S2-b, Supporting Information). The resulting nanoparticles are designated as "MSN-*y*PEG".

In order to unambiguously demonstrate the efficient grafting of Gd-DTPA and PEG, the new MSNs derivatives were systematically characterized after each step using solid state NMR, FTIR, N_2 physisorption and XPS measurements. **Figure 2** shows the ^{13}C CP NMR data for MSN-*x*DTPA and MSN-*y*PEG. Characteristic peaks for DTPA-silane and PEG-silane were revealed for all MSN-*x*DTPA and MSN-*y*PEG particles, respectively. Indeed, the ^{13}C CP MAS NMR spectrum of MSN-*y*PEG (Figure 2-a and Figure S3-a, Supporting Information) showed a typical peak at 70 ppm, which was assigned to ethyl carbons O–$(CH_2CH_2–O)_n$.[29] Resonances of the remaining ethoxy groups in the –Si–O–CH_2CH_3 groups appeared at 59 ppm and 15 ppm. All of the ^{13}C CP/NMR spectra of the MSN-*x*DTPA samples (Figure 2-b and Figure S3-b, Supporting Information) showed sharp resonances for all DTPA-silane-related carbon atoms (peak attributions are displayed in Figure 2).

The presence of grafted DTPA-silane and PEG-silane molecules was further confirmed by FTIR spectroscopy. The MSN-*x*DTPA spectra (Figure S4-a, Supporting Information) showed the asymmetrical C = O vibration of –COOH at 1719 cm^{-1} and exhibited also a very weak band (as a shoulder) at 1670 cm^{-1}, characteristic of the amide band.[30] The symmetrical C-H stretching vibrations of $–CH_2$, as well as their deformation vibration ($\delta_{C\text{-}H}$) were visible at 2920 and 1389 cm^{-1}, respectively. The presence of PEG-silane in grafted MCM-48, was evidenced by symmetrical and asymmetrical C-H stretching vibration bands of $–CH_2$ in the 2800 and 2995 cm^{-1} frequency range. The $\delta_{C\text{-}H}$ vibrations and the bending vibrational modes (scissoring) of the CH_2 group were also noted at 1349, 1455 and 1472 cm^{-1}, respectively (Figure S4-b, Supporting Information). As expected, ^{29}Si MAS NMR spectra of all the samples (MSN-*x*DTPA and MSN-*y*PEG) depicted a broad multicomponent peak in the –88 to –120 ppm range, which is associated with the Q^n groups of the silica framework ($Si(OSi)_n(OH)_{4-n}$; n: [1–3]) (Figure S5, Supporting Information). For samples with high percentages of grafted molecules (>9% for DTPA-silane and >10.5% for PEG-silane), moderate intensity resonances were observed around [-57 – -67] ppm (Figure S5, Supporting Information; j, k, m, n). These signals were attributed to T^n groups ($(C\text{-}Si(OSi)_n(OH)_{3-n})$ of the covalently grafted PEG-silane molecules. The grafting of PEG-silane and DTPA-silane on MCM-48 was successful, as confirmed by NMR and IR.

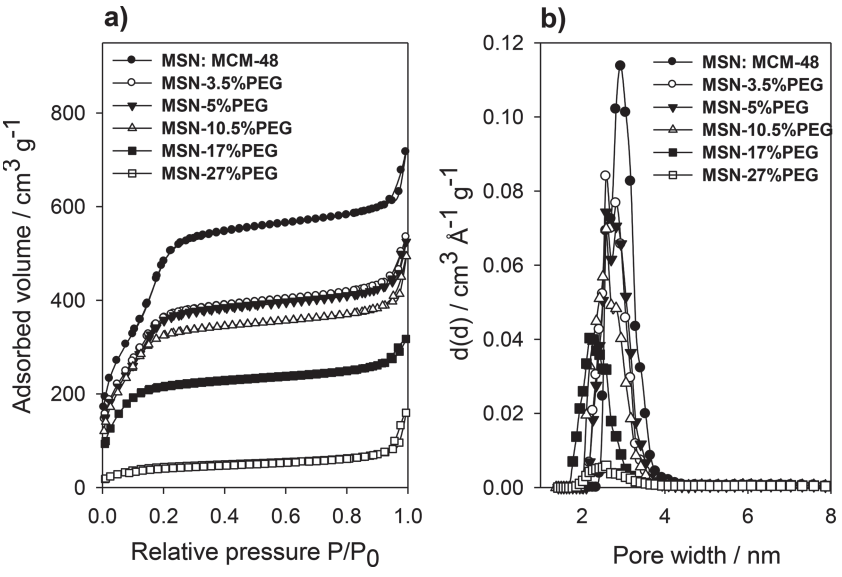

Figure 3. N_2 physisorption isotherms a) and respective NLDFT pore size distributions b) of MSN-*x*PEG nanoparticles.

MSN-*y*PEG with $x \leq 10.7\%$ are mesoporous materials, as confirmed by their N_2 physisorption Type IV isotherms (**Figure 3**-a). These isotherms are similar to those observed for pristine MCM-48. On the other hand, MSN-*y*PEG samples with x > 10.7% show isotherms belonging to type I category (that is, microporous materials) (Figure 3-b), indicating a reduction in the pore size upon grafting with high amounts of PEG-silane. The results suggest an excessive coverage of PEG chains at the entrance of the mesopore channels, which might affect the diffusion of nitrogen inside the pores. Increasing concentrations of PEG-silane used at the grafting step, resulted in higher PEG-related %C content as estimated from XPS: from 4.5 to 6.2 to 9.6%C for MSN-3.5%PEG, MSN-5%PEG and MSN-10.5%PEG, respectively (data not shown). Because XPS is a surface analysis technique (analysis depth around 5 nm), this fact is in line with the preferential accumulation of PEG at the exterior surface of MSNs when high concentrations of PEG are used for the grafting. Therefore, the weight loss observed in TGA for high PEG-silane (>10.7%) is most likely attributed to PEG accumulated at the entrance of the mesopores, and attached at or close to the outer surface of MSNs.

Porosity data obtained from the analysis of MSN-*y*PEG nanoparticles are reported in **Table 1**. For the high percentages of grafted PEG-silane (>10.7%), the values for surface areas and pore volumes decreased considerably (from 1650 to [792–166] $m^2\ g^{-1}$) while the pore sizes were reduced from 3 down to 2 nm. However, in the case of small amounts of PEG-silane (≤5%), more than 84% of the surface area and pore volume were conserved. In that case, pore sizes decreased slightly from 3 to 2.7 nm. It is important here to note that the grafting of small percentages of high-molecular-weight PEG-silane (10 and 20 kDa) on MSNs is sufficient to minimize the phagocytosis of MSNs by the mononuclear phagocyte system, as previously reported.[11a]

The textural properties of MSN-*x*DTPA samples are summarized in Table 1. These data show that the higher the percentage of grafted DTPA-silane, the lower are the surface area and pore volume. Consequently, grafting of only small amounts of DTPA-silane or PEG-silane (≤ 5.7%), ensures the conservation of at least 90% of the MSN surface area and pore volume. Furthermore, the mean pore diameters of these nanoparticles are almost identical to that of the parent MCM-48 (Table 1 and Figure S6, Supporting Information). Thus, the porosity data of MSN-*x*DTPA and MSN-*y*PEG indicate that low percentages of PEG-silane and DTPA-silane (< 6%) ensure a selective grafting of the outer surface of MSNs, preventing the deleterious occlusion of the pores that could impede drug loading. This result could be explained by two phenomena: (1) first, adsorption sites are more readily accessible on the outer surface of

Table 1. Physicochemical parameters of MSN-*y*PEG; MSN-*x*DTPA and MSN-*x*DTPA-*y*PEG nanoparticles extracted from nitrogen physisorption measurements.

		BET Surface Area [$m^2\ g^{-1}$]	Pore Volume [$cm^3\ g^{-1}$]	NLDFT Mean Pore size [nm]
MSN	MCM-48 (pristine)	1654	0.82	3
	MSN-3.5%PEG	1471	0.70	2.7
	MSN-5%PEG	1448	0.68	2.7
MSN-xPEG	MSN-10.5%PEG	1267	0.60	2.4
	MSN-17%PEG	792	0.41	2.1
	MSN-27%PEG	166	0.12	2.1
	MSN-3%DTPA	1500	0.74	3
MSN-yDTPA	MSN-9%DTPA	1393	0.68	3
	MSN-5.7%DTPA	1603	0.74	3
	MSN-13%DTPA	1083	0.52	2.9
MSN-DTPA-PEG	MSN-5.7%DTPA-3.2%PEG	1530	0.74	3

the nanoparticles; (2) diffusion of molecules into the pores is considered negligible owing to the low concentration of both DTPA-silane and PEG-silane,[31] as well as to the high molecular weight of PEG-silane (20 kDa).

The next step consisted in the design of MSNs grafted with both molecules. This was carried out by presenting 3.2% of PEG-silane to MSN-5.7%DTPA nanoparticles. As shown in Table 1, for this preparation, more than 90% of the initial porous volume was conserved after functionalization. The final nanoparticles (MSN-5.7%DTPA-3.2%PEG) are characterized by high surface area (1530 m^2 g^{-1}) and high pore volume (0.74 cm^3 g^{-1}). These values are similar to those measured for pure MSNs (MCM-48).

The present study demonstrates the key importance of grafting the smaller compounds (DTPA-silane), prior to grafting long molecules (e.g. PEG-silane, 20 kDa). This sequence prevents the occurrence of a strong competition between the two molecules, and ensures control and reproducibility to the procedure. Indeed, by presenting DTPA-silane to a preparation of MSN-γPEG (γ = 3.5 and 5%), we demonstrated the inhibition of DTPA-silane grafting, most probably due to the presence of the large PEG molecules (20kDa) crowding the outer surface of nanoparticles. In fact, only 1.5% (w/w) of DTPA-silane could be grafted using this reaction sequence (regardless of the initial amount of DTPA-silane added). Moreover, when presenting DTPA-silane to MSNs after grafting of high molecular weight PEG-silane, DTPA-silane molecules seemed attached into/at the entrance of the pores (Table S1, Supporting Information). In contrast, by reacting the smaller molecules first (DTPA-silane), it became possible to take advantage of the few un-reacted silica surface regions remaining available for the attachment of PEG-silane. Indeed, after the grafting of 5.7% DTPA-silane, only 3.2% of PEG-silane were grafted at the outer surface without pore obstruction. This relatively low percentage attributed to PEG-silane (20 kDa) is however sufficient and considered like an optimal weight percentage to minimize non-specific protein adsorption at the surface of MSNs and PEG-MSNs phagocytosis. In fact, it has been observed that, as low is the percentage of grafted high molecular weight PEG-silane (20 kDa), as low the non-specific protein adsorption (human serum protein) and the phagocytosis of MSNs by macrophages (with particle sizes of 150 nm).[11a]

Thus, the experimental protocol developed in the present study allowed for the first time the conservation of 92% of surface area, 90% of pore volume and 100% of pore diameter of MCM-48 nanoparticles, after grafting of PEG and DTPA molecules. This is a significant advance in the preparation of MSNs for drug delivery, since preservation of high pore volume is needed to achieve high drug loads. The presence of both DTPA and PEG on the grafted MSNs was demonstrated by NMR and FTIR: all peaks and bands characteristic of both DTPA-silane and PEG-silane were clearly revealed in ^{13}C CP NMR and FTIR spectra (MSN-5.7%DTPA-3.2%PEG, Figure S7, Supporting Information). In addition, the successful grafting of PEG-silane and DTPA-silane at the outer surface was also confirmed by X-ray photoelectron spectroscopy (XPS) analysis with emphasis on O (1s), Si (2s), C (1s) and N (1s). Indeed, the XPS data (Table S2, Supporting Information) revealed a significant increase in the carbon atomic percentage (%C) and carbon-to-silicon ratio (C/Si) from 6.2% and 0.235, for the MSN-5.7%DTPA sample, to 8.6% and 0.332 after PEG-silane grafting, respectively. Moreover, the percentage of nitrogen (%N) only increased slightly (up to 0.8%) after DTPA-silane grafting. It remained the same after PEG-silane grafting. Furthermore, a nitrogen-to-silicon ratio (N/Si) of about 0.03 was found after DTPA-silane grafting. This corresponds perfectly to the theoretical N/Si molar ratio calculated from the grafted percentage (w/w) of DTPA-silane. Because XPS detects the presence of elements in a maximum depth of a few nanometers only, this exact same N/Si ratio is in line with the presence of DTPA-silane molecules grafted at the outer surface of MSNs. To compare with the XPS data, the elemental ratios of nanoparticles in which Gd^{3+} ions are complexed, were also measured by energy dispersive X-ray spectroscopy (EDX, coupled on a HRTEM system). While XPS provides elemental ratios from the first nm depth in the surface, EDX can here provide information from the entire volume of electron attenuation (this corresponds more or less to the "bulk" volume of MSNs). By focusing the electron beam at the core of the particles, and then at the outer boundary of MSNs, it was possible to perform a comparative elemental ratio study (Gd/Si). With XPS, Gd/Si ratios of 0.03 were found, and these were almost exactly the same as those found with EDX at the outer boundary of MSNs (0.034). However, indications of strong segregation were found when the measurement was performed at the core of MSNs ("bulk" Gd/Si = 0.015). One has to keep in mind that the electron beam reaching the core of MSNs, also crosses the outer surface twice, and therefore the EDX spectrum is invariably contaminated by Si and Gd signals from the exterior of the particles. Nonetheless, the much lower Gd/Si ratio found by focusing the electron beam at the core of MSNs, confirms the strong segregation of Gd at the exterior of the silica particles compared to the composition of their core.

2.2. ^1H Relaxometric Properties

The relaxometric properties of Gd(III)-chelated MSN-5.7%DTPA-3.2%PEG were measured in nanopure water, using a dedicated NMR relaxometer (1.41 T). The relaxation rates ($1/T_1$ and $1/T_2$) were then plotted in function of the Gd^{3+} concentration values (measured by ICP-MS). As shown in **Figure 4**-a, the slope of relaxivity curves ($1/T_{1,2} = r_{1,2}$ ([Gd^{3+}] + C) provided the relaxivity values (r_1, r_2), which are used to normalize and compare the performance of MRI contrast agents. Indeed, high r_1 values indicate the potential of Gd-based paramagnetic contrast agents to induce "signal brightening". Because the relaxivities are calculated by normalizing the relaxation rates to the concentration of Gd^{3+} ions in the compound, the performance of Gd(III)-chelated MSN-5.7%DTPA-3.2%PEG can be directly compared to that of commercial contrast agents such as Gd-DTPA. In this way, it is a very quantitative measurement of the "brightness" of the particles in T_1-weighted MRI. Also, paramagnetic "positive" contrast agents must present r_2/r_1 ratios as low as possible (e.g. 1.1 for Gd-DTPA), in order to minimize the loss of phase coherence that result in the decrease of the transversal relaxation rates.[32] This is the case for suspensions of MSNs that present a too strong con-

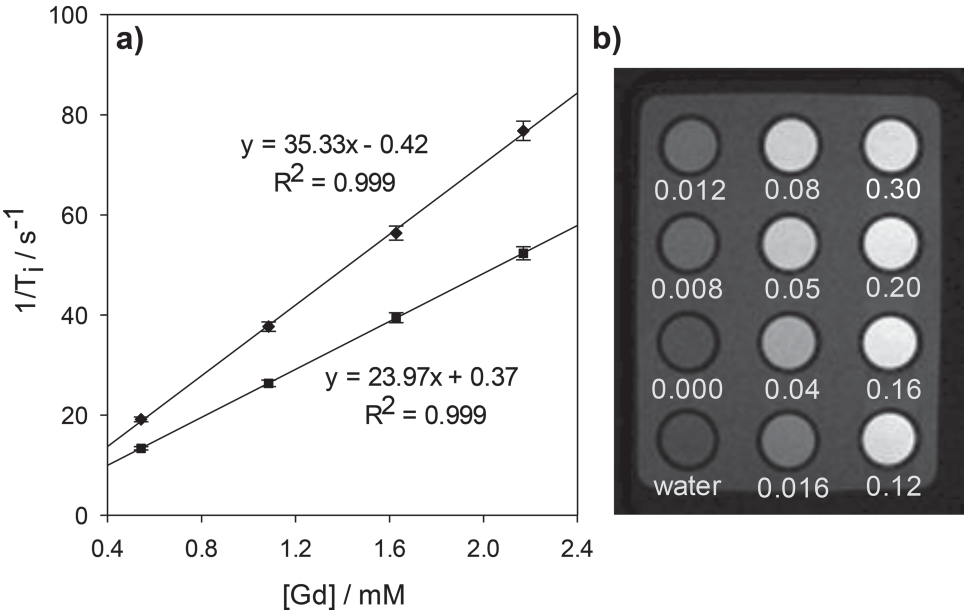

Figure 4. a) Longitudinal ($1/T_1$ + C, squares) and transverse ($1/T_2$ + C, diamonds) relaxation rates of MSN-5.7%DTPA(Gd)-3.2%PEG nanoparticles, in function of Gd^{3+} concentration values; b) T_1-weighted MR images of MSN-5.7%DTPA(Gd)-3.2%PEG nanoparticles measured at clinical magnetic field strength (1 Tesla, TE/TR = 10.7/1000 ms). Numerical values indicate the Gd concentrations (mM) measured by ICP-MS.

centration of Gd^{3+} ions. At 37 °C, the following relaxivities were found for Gd(III)-chelated MSN-5.7%DTPA-3.2%PEG: r_1 = 23.97 mM^{-1} s^{-1}; r_2 = 35.33 mM^{-1} s^{-1}; r_2/r_1 = 1.47. Compared with the previously reported Gd-MSNs products, where no apparent attempt was made to optimize the number of Gd^{3+} ions per MSNs, the Gd-loaded nanoparticles developed in this work exhibit the lowest r_2/r_1 ratio reported thus far for all Gd-loaded MSNs materials.[14c,d,17,33] It therefore bears the highest potential as a "positive" MRI contrast agent among MSN-based compounds. This study also confirms the importance of a careful balance of Gd^{3+} ion load per nanoparticle to achieve high relaxometric performances. The signal-enhancement performance of Gd(III)-chelated MSN-5.7%DTPA-3.2%PEG nanoparticles was clearly demonstrated by scanning dilutions of this product in 1Tesla MRI (Figure 4-b). *In vitro* T_1-weighted MR images confirmed the possibility to achieve remarkable positive contrast enhancement even at very low Gd concentrations. Precisely, a positive contrast enhancement of at least 105% could be achieved even at the following concentrations: [Gd] = 0.04 mM and [Si] = 1.26 mM, as confirmed by ICP-MS. According to these data, 0.428 nmol nanoparticles per litre is a sufficient concentration to reach a detectable contrast enhancement in 1 T MRI. Such an optimal performance is attributed to the presence of Gd-DTPA moieties selectively grafted at the outer surface of the mesoporous silica particles (EDX data, see section 2.1). This facilitates the exchange of water bound to the Gd^{3+} complexation site, with water from the environment (matrix). Recently, Carniato et al.[14b] reported that water molecules have a limited diffusion through the pores of MSNs. Therefore, for optimal relaxometric properties, anchoring Gd-chelates at the outer surface of MSNs is an essential criteria, and the results of the present study are in line with this theory. Also, the presence of Gd^{3+} ions sequestrated at the exterior surface of the particles, far from the rotational axis of the particles, is expected to have a strong impact on the rotational correlation time of the contrast agent. In fact, this is one of the main factors guiding their relaxometric performance.[34] In general, aqueous suspensions of large particles and low tumbling rates, produce higher longitudinal relaxivities. In summary, strong interactions between water and the paramagnetic functions, as well as a selective grafting of Gd at the outer surface of particles, is a sound strategy to optimize the relaxometric performance of the contrast agent while minimizing the use of potentially toxic Gd^{3+} ions.

In addition, we have studied the stability of Gd^{3+} chelation and the potential release of Gd^{3+}-DTPA from the MSNs surfaces. For this, MSN-5.7%DTPA(Gd)-3.2%PEG nanoparticles were suspended in PBS pH 7.4 and in acidic buffer (pH 5), using a dialysis membrane (1000 MW, Spectra/Por #6). Samples of the dialysate were taken at time points, followed by ICP-MS analysis. The results, depicted in Figure S8, Supporting Information, revealed that, very low amounts of free Gd^{3+}, or Gd^{3+}-DTPA were found in the dialysates after 24h (0.36–0.42%) with respect to the initial Gd^{3+} concentration in the colloidal suspension. After 9 days (216 hours), the release rate levelled-off to values in the range (1–2%), i.e. more than 98% of initial chelated Gd amount remained attached to the MSNs. Such results indicate that chelated Gd^{3+} ions are strongly bound to the nanoparticles, and therefore the contrast-enhancement effects detected in MRI would be directly attributed to the presence of MSNs.

2.3. Colloidal Stability

Biomedical applications require the development of particles that form stable colloids in physiological conditions. In fact, aggregation phenomena could harm the efficacy of such

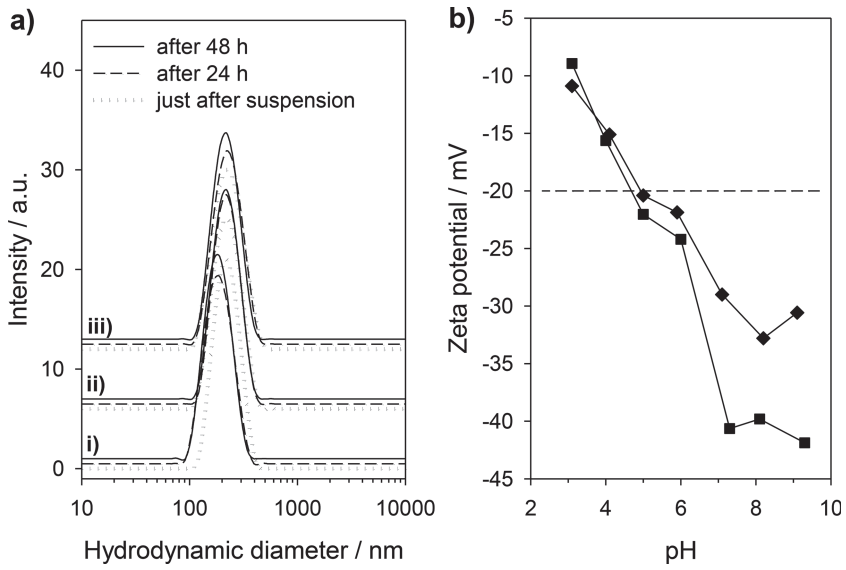

Figure 5. a) DLS analysis of MSN-5.7%DTPA(Gd)-3.2%PEG suspension in: water (i), SBF (ii) and in cell culture medium (iii); b) zeta potential dependence on pH for MSN-5.7%DTPA-3.2%PEG before (squares) and after (diamonds) Gd chelation.

materials and be deleterious to the patients.[1f] Preserving the colloidal stability of the MSNs designed for drug delivery is a major issue in the field. For this, the colloidal stability of MSN-5.7%DTPA(Gd)-3.2%PEG nanoparticles was investigated and monitored by dynamic light scattering (DLS). Hydrodynamic diameter measurements were carried out in aqueous suspension as well as in simulated body fluid (SBF) and in culture medium (DMEM + serum). Hydrodynamic diameter distributions are shown in **Figure 5**-a. Intensity-weighted data are represented to facilitate the detection of any sign of aggregation or flocculation. MSN-5.7%DTPA(Gd)-3.2%PEG nanoparticles formed a stable colloidal solution with a hydrodynamic diameter of ≈190 nm in water suspension and around 225 nm and 229 nm in simulated body fluid and culture medium, respectively. No evidence of agglomeration or flocculation was found and no significant increase in hydrodynamic diameter was reported at least up to 48 hours, confirming the excellent colloidal performance that these systems could have in physiological media. In addition, zeta potential analysis revealed a strongly negative surface charge value ≤ –20 mV at pH ≥ 5 (Figure 5-b). This confirmed the adequate colloidal stability of these nanoparticles in a large range of physiological pH conditions, making these particles suitable for in vitro and in vivo biomedical applications.

2.4. Biocompatibility and Viability Test

To assess the biocompatibility of the developed nanocarriers, *in vitro* cytotoxicity tests were performed by incubating P388 cells with suspensions of MSN-5.7%DTPA-3.2%PEG and MSN-5.7%DTPA(Gd)-3.2%PEG (concentrations from 0 to 100 μg mL^{-1}) for 24 h and 48 h, and using trypan blue (cell death) and resazurin (cell proliferation) cell viability essays. P388 cells are strongly phagocytic and they have already shown their capacity to provide an excellent uptake of MSNs with a mean size of 150 nm.[35] Because MSNs are designed to be administrated intravascularly, it is rational to demonstrate the cell viability by using such a phagocytic white blood cell line. As shown in **Figure 6**, no cell death and no significant growth inhibition were found at all concentrations, up to 100 μg mL^{-1}. The preservation of cell viability suggests that both MSN-DTPA-PEG and MSN-DTPA(Gd)-PEG nanoparticles are biocompatible nanocarriers.

2.5. Drug Loading and In Vitro Drug Release

The capacity of MSN-5.7%DTPA-3.2%PEG nanoparticles to entrap and release anticancer agents was demonstrated with daunorubicin (DNR). Such studies were performed to highlight the potential of MSN-DTPA-PEG nanoparticles for theranostic applications. The presence of DNR in the loaded particles was evidenced by ^{13}C CP/NMR and FTIR (Figure S8, Supporting Information). The DNR adsorption capacity of Gd-labeled nanoparticles (MSN-5.7%DTPA(Gd)-3.2%PEG) was in the order of 8% (w/w) which is two to six times higher than those of typical MSNs used thus far in previous drug delivery studies (e.g., MCM-41-type).[4c,i] According to this percentage, the amount of loaded DNR is equal to 0.08 mg per mg of nanoparticles which corresponds to 150 nmol of DNR per mg of nanoparticles. Such enhanced drug adsorption capacities are attributed to the high surface area and the high pore volume of the DTPA-and-PEG-grafted MCM-48. Indeed, compared to MCM-41 showing a two-dimensional (2D) pore network, MCM-48 nanoparticles are characterized by higher surface area and easier molecular diffusion inside their open three-dimensional (3D) pore network.[36] Moreover, the drug loading efficiency of MSN-DTPA(Gd)-PEG nanoparticles is attributed to the noncovalent bonds (e.g. electrostatic interactions and hydrogen bonding) between the amine group of DNR and adsorption sites at the surface of silica (e.g. silanol and siloxane groups). According to the loading conditions of DNR, DNR adsorption in the silica nanoparticles could be attributed to electrostatic interactions taking place between positively charged DNR ($DNRH^+$) molecules and deprotonated silanol groups (SiO^-), as well as to hydrogen bonding occurring between uncharged DNR and the silica framework (silanols and siloxane groups).

The drug release efficiency was investigated *in vitro* in PBS pH 7.4, and in acetate buffer solutions pH 5 and pH 4, which are conditions often used to mimic *in vivo* media. **Figure 7**-a,b depicts the cumulative DNR release for MSN-DTPA(Gd)-PEG nanoparticles as a function of time. In acidic conditions, a progressive drug release was observed in the first 24 hours (about 9.5–12.5 nmol per mg of nanoparticles). After 9 days, the cumulative release of DNR reached 11 and 14 nmol per mg nanoparticles in pH 5 and pH 4, respectively. These concentrations are five and six times higher than that observed in PBS at pH 7.4, respectively. Indeed, at pH 7.4, a very slow drug release rate was observed, with the plateau occurring around 150 h (6 days) after beginning of the experiment. These are demonstrations that drug release can be achieved in a time

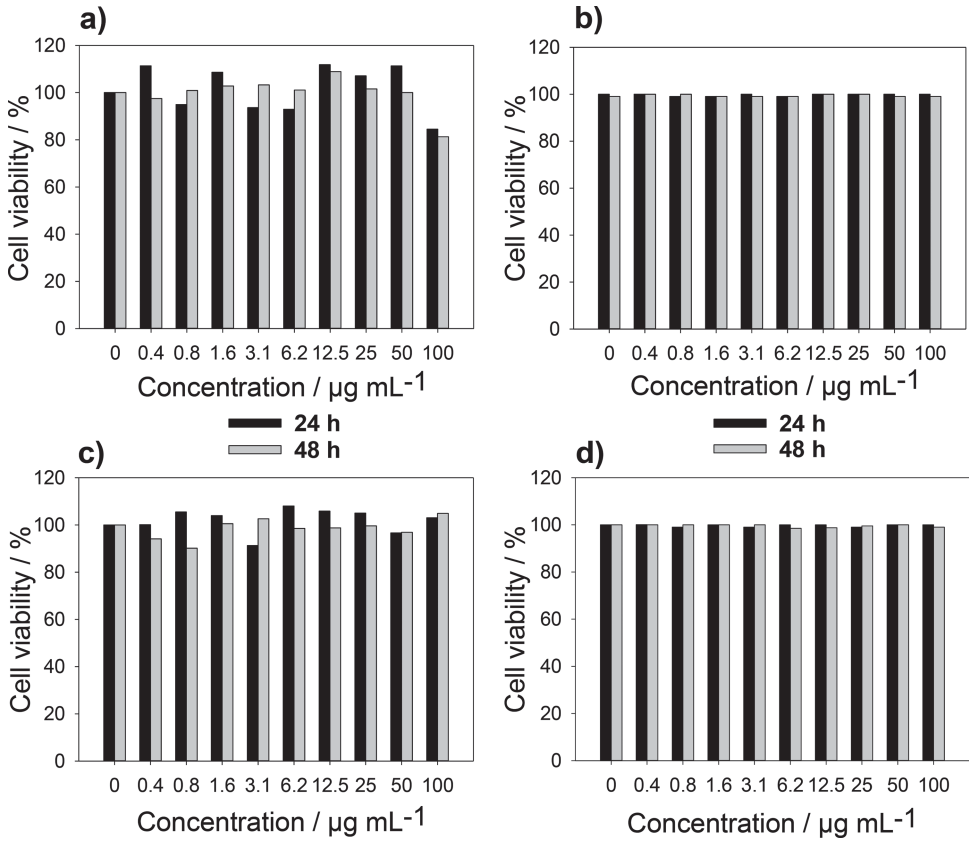

Figure 6. Cell viability assay of P388 cells treated with MSN-5.7%DTPA-3.2%PEG (a: resazurin test; b: trypan blue test) and MSN-5.7%DTPA(Gd)-3.2%PEG (c: resazurin test; d: trypan blue test).

and pH-dependent manner. The low release level at pH 7.4 and the higher values achieved under more acidic conditions, are related to the electrostatic interactions between silica adsorption sites (silanol groups) and daunorubicin. Indeed, when DNR@MSN-DTPA(Gd)-PEG nanoparticles are suspended in acidic solution, the SiO^- groups of silica framework become protonated (SiOH), inducing the liberation of protonated DNR ($DNRH^+$) and, thus, the observed release. However, when these

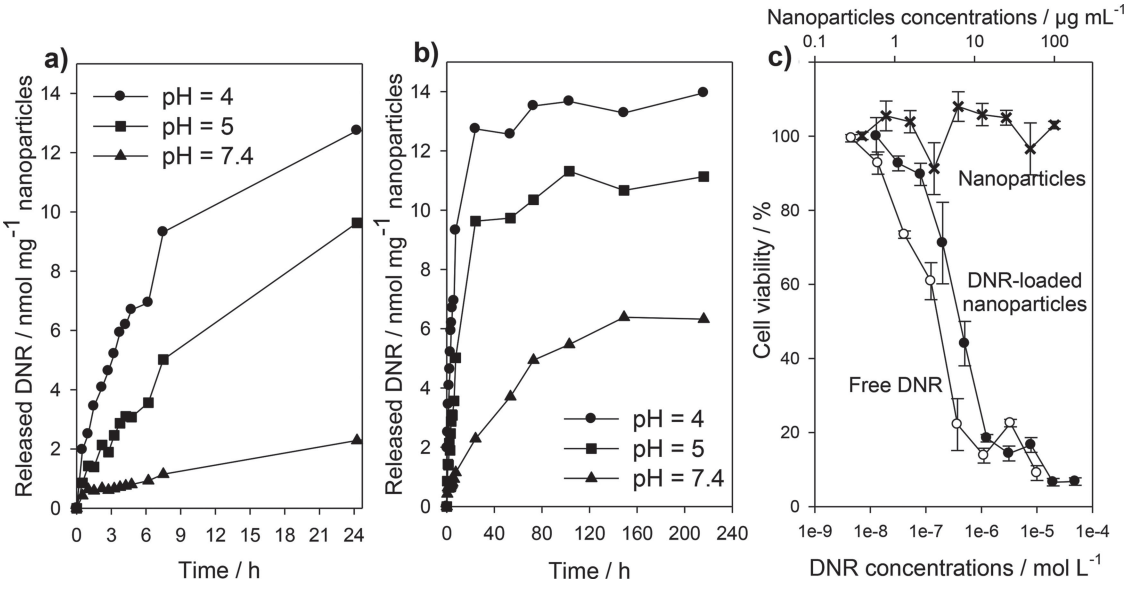

Figure 7. Daunorubicin release from MSN-5.7%DTPA(Gd)-3.2%PEG nanoparticles as a function of: a) initial time up to 24 h (1 day); b) total time up to 216 h (9 days) and c) viability of P388 cells incubated with free DNR, DNR-loaded nanoparticles at different DNR doses, and non-loaded MSNs.

nanoparticles are suspended in neutral solution (e.g. PBS pH 7.4), the predominant silanol species are mostly SiO^-, which more strongly interact with positively charged protonated DNR ($DNRH^+$). This proton-sensitive mechanism indicates the possibility to trigger intracellular drug release once the particles are internalized in cells, enabling the intracellular accumulation of very high amounts of drugs,[4c] ultimately enhancing drug efficiency and reducing deleterious effects of free anticancer agents.[4i,5b]

In order to identify in a quantitative manner evidence of mechanisms that have a potential on drug desorption and release kinetics, *in vitro* release data (DNR@MSN-DTPA(Gd)-PEG) were fitted using a semi-empirical power law equation[37]:

$$\frac{M_t}{M_\infty} = k \times t^n \quad (1)$$

where: M_t is the amount of the drug release at time t (in hours);
M_∞ is the total amount of the loaded drug;
k is the kinetic release constant and
n is a release factor

The k value in **Equation 1** provides information on the release rate and the n value indicates the type of drug release mechanism.[37] Both values (n and k) were calculated from the plot of $\log\left(\frac{M_t}{M_n}\right) = f(\log t)$ and compiled in Table S3, Supporting Information. The release exponent (n) in the more acidic medium (pH = 4), equals to 0.5, and thus presented pure Fickian diffusion, whereas in higher pH medium (pH = 5 and pH = 7.4), the release exponent shifted to values higher than 0.5 (Table S3, Supporting Information), indicative of a combination of both diffusion and erosion-controlled rate release.[37] Such so-called "erosion" release was previously attributed to the degradation behavior of calcined, uncalcined and PEGylated silica nanoparticles in simulated biological medium as discussed by Shi et al.,[38] Bein et al.[13a] and Kuroda et al.,[39] respectively. This further explains why in PBS at pH 7.4, the results showed a slow and continuous release over a 9-day period. On the other hand, as shown in Table S3, Supporting Information, the kinetic constant (k) value is quite low. This indicates progressive and prolonged release behaviour over time that could be truly useful to enhance the long-term anticancer drug efficacy and may achieve improved therapeutic efficacy.

The drug release studies were completed with a cell viability study. For this, P388 cells were incubated 24 h with DNR-loaded nanoparticles and the viability was measured at time points (Figure 7-c). Significant inhibition of cell growth and proliferation were observed for DNR-loaded nanoparticles, while no significant cytotoxicity was observed with unloaded nanoparticles (free of daunorubicin). Moreover, the cytotoxicity efficacy of the DNR-loaded nanoparticles was similar to that of free DNR dissolved in DMSO, at equal concentrations of daunorubicin. DNR is efficiently released in the intracellular medium after cell uptake.

Finally, the present study clearly reveals one potential challenge intrinsic to MSNs as delivery vectors: adsorption mechanisms taking place between the medicinal compounds and the pore surfaces of the silica framework. Indeed, the concentration of released DNR drug reported in this study is comparable to those of the literature[4f,i] which, in our case, represents 8–10% of the initially loaded drug. However, higher released drug concentrations and cumulative drug release were expected in the present study, due to the exceptional drug loading capacity of this system. Our results suggest the occurrence of strong interactions taking place between DNR and the silica matrix. Investigations are currently being performed to fully understand and control the exact adsorption/desorption mechanisms between the drug and the silica matrix. This would be a critical information since this phenomenon has also been suggested by recent studies,[25] and because DNR is a widely used anticancer molecule in drug delivery studies. The level of drug release achieved in the present study is nonetheless very effective to control cell growth, as shown by the cytotoxicity results.

3. Conclusions

This contribution is the first study that confirms the optimal combination of relaxometric performances and drug adsorption/release capacity of MSN-based drug vectors labeled with metal chelates. The selective grafting of imaging probes (DTPA-Gd) and biocompatible molecules (PEG) at the outer surface of the particles is a straightforward strategy to preserve the high porosity of MSNs (a critical parameter for drug delivery function). The very small amounts of the MRI probe molecule, i.e., Gd-chelate, grafted at the outer surface induces strong relaxometric properties and remarkable positive contrast enhancement in MRI. Owing to the conservation of the porosity, the obtained multifunctional nanoparticles offer also the advantages of nanocarriers with high drug loading capacity (demonstrated with daunorubicine, an anticancer drug model). The pH-responsiveness of the nanocarriers and their high colloidal stability were illustrated, which opens promising applications in tumour drug delivery applications. This study is a significant and original step toward the development of tailored theranostic nanocarriers using high porosity MSNs.

4. Experimental Section

4.1. Materials

Tetraethylorthosilicate (TEOS, 98%), n-cetyltrimethylammonium bromide (CTAB, 99%), Pluronic F127 ($EO_{106}PO_{70}EO_{106}$, BioReagent), diethylenetriaminepentaacetic dianhydride (DTPA dianhydride, 98%), (3-aminopropyl)triethoxysilane (APTES, 99%), $Gd(CH_3CO_2)_3{,}xH_2O$ (99,9%) were obtained from Sigma-Aldrich (Canada) in high purity grade. Polyethylene glycol (PEG-Silane 20 kDa) was purchased from Laysan Bio (Arab, USA).

4.2. Mesoporous Silica Nanoparticles Synthesis

MCM-48-type MSNs with 3-D cubic network, were synthesized as reported in the literature.[27] Briefly, CTAB (1.0 g) and F127 (4.0 g) were dissolved in EtOH 100% (85.41 mL) and 2.8 wt% NH_4OH solution (212.86 mL). Then, TEOS (3.86 mL) was added at room temperature (RT) under high stirring rate (1000 rpm) for 1 minute. The reaction mixture was then aged 24 h in static conditions (air, RT). The resulting

product was collected by centrifugation, washed twice with EtOH 95% (250 mL) and dried overnight in air at 65°C. Finally, the product was calcined (air, 550 °C, 1 °C min^{-1}, 5h).

DTPA Grafting Optimization: In a flask, DTPA dianhydride (200 mg, 0.56 mmol) was dissolved in anhydrous DMSO (at RT, 3 h stirring and 5 min sonication). Then, APTES (0.1 mL, 0.45 mmol) was added dropwise (for optimum reactivity) and the mixture was stirred overnight at RT, under N_2. This product was referred to as "DTPA-silane solution". In another flask, calcined nanoparticles (500 mg) were suspended in anhydrous toluene (85 mL) and sonicated for at least 30 min. Varying amounts of the DTPA-silane solution (x = 3, 2, 1 and 0.5 mL) were added one shot to the nanoparticle suspension under inert gas (N_2) and the mixture was refluxed overnight at 110 °C. The suspension was centrifuged (7500G, 10 min), and the supernatant discarded. The solid residue was washed twice with EtOH 95%, once with water, and dried under vacuum at 40 °C. The resulting nanoparticles are designated as "MSN-*x*DTPA", where *x* is the w/w percentage of grafted DTPA-silane measured by TGA (Figure S2-a, Supporting Information).

PEG Grafting Optimization: escalating amounts of PEG-silane (y = 30, 20, 10, 5 mg) were dissolved in anhydrous toluene (15 mL) at RT under inert gas (N_2), followed by 6 h stirring and 10 min of sonication. The PEG-silane solution was then added to the suspension of calcined nanoparticles (300 mg in 85 mL dry toluene) and the final suspension was refluxed under N_2 overnight at 110 °C. The product was isolated by centrifugation (7500G, 10 min), washed twice with EtOH 95%, once with water, and dried under vacuum at 40 °C. The resulting nanoparticles are designated as "MSN-*y*PEG" where *y* is the w/w percentage of grafted PEG-silane as measured by TGA (Figure S2-b, Supporting Information).

DTPA-Gd(III) Chelation: $Gd(CH_3CO_2)_3{,}xH_2O$ (1 mL, 100 mM) was slowly added to the nanoparticles (10 mg). The obtained suspension was stirred under moderate agitation (60 min, RT). The labeled particles were recovered by centrifugation (7500G, 10 min). These nanoparticles were washed once with sodium acetate buffer (10 mL, 50 mM) and several times with nanopure water (10 mL). Between each washing, the T_2 of the supernatant was measured with a dedicated TD-NMR relaxometer (Bruker Minispec 60 mq, 60 MHz, 25 °C). When T_2 reached 2300 ms, the supernatant was considered Gd^{3+}-free and the particles were then considered purified from un-chelated Gd^{3+} ions. Finally, Gd-labeled nanoparticles "MSN-*x*DTPA-*y*PEG(Gd)" were dried overnight under vacuum at 40 °C. The successful chelation of gadolinium was confirmed by IR spectroscopy, based on the disappearance of the asymmetrical C = O vibration of –COOH at 1719 cm^{-1}, and the appearance of the typical vibration mode of DTPA(Gd) at 1591 cm^{-1}, corresponding to asymmetrical COO^- stretching vibration.[40]

4.3. MSNs Textural Properties and Thermogravimetric Analysis

X-ray Diffraction Characterization: XRD measurements were performed using a Siemens D5000 (reflection, θ–θ configuration; $Cu_{K\alpha}$: λ = 1.541 Å; 40 kV; 30 mA; 1–8° 2θ, step size: 0.02 2θ; 0.02 s/step). The Jade (v 2.1) software coupled with JCPDS and ICDD (2001 version) databases was used to analyze the XRD data.

Nitrogen Physisorption Analysis: Nitrogen physisorption measurements were performed at –196 °C with an ASAP 2010, Micromeritics. Before the sorption measurements, the samples were outgassed under vacuum for at least 6h at 200 °C (for calcined MCM) or 80 °C (for all the functionalized MSNs). The specific surface area (S_{BET}) was determined using the BET equation in the range $0.05 \geq P/P_0 \geq 0.20$ and the total pore volume was obtained at $P/P_0 = 0.95$. Pore diameter was estimated using non-local density functional theory (NLDFT) methods (Autosorb 1.55 software, Quantachrome Instrument) applying adsorption branch model (considering N_2 sorption at –196 °C in silica with cylindrical pore geometry).

Thermogravimetric Analysis-Differential Thermal Analysis (TGA-DTA): Measurements were performed using a Netzsch STA 449C thermogravimetric analyzer, under airflow of 20 mL min^{-1}, with a heating rate of 5 °C min^{-1}, between 35 and 700 °C. The percentage of grafted molecules (DTPA-silane/APTES and PEG-silane) was calculated based on the mass loss detected between 160 °C and 530 °C. This temperature range was selected because the degradation of PEG-silane and DTPA-silane takes place between 180 and 500 °C, and because it excludes from the calculation the residual solvent (e. g. physisorbed water) and the silica framework condensation occurring further at higher temperatures.

4.4. Particle Size and Physicochemical Analysis

TEM and EDX Characterization: The nanoparticles were dispersed in methanol. This suspension (4 µL) was deposited on a carbon-coated copper grid and images were taken in TEM (JEM-1230) at an accelerating voltage of 80 keV. Particle size distributions were calculated by ImageJ, based on a sample of at least 1500 particles, from at least 6 images taken over 6 different quartiles. The Gd/Si ratio in MSN-5.7%DTPA(Gd)-3.2%PEG nanoparticles was measured with energy dispersive X-ray spectroscopy (EDX) analyses, performed with a high resolution TEM (JEOL JEM-2100F, 200 keV).

Particle Size and Zeta Potential Measurements: The hydrodynamic diameter of the nanoparticles and the zeta potential were measured by dynamic light scattering (DLS), using a Malvern DTS Nano zetasizer 173° (equilibration time set to 3 min; 3 measurements taken on each sample; only quality criteria data accepted as valid results). Zeta potential dependence on pH was obtained by measuring the zeta potential in aqueous solution by adjusting the pH value by the addition of HCl and NaOH (0.02 M).

NMR Characterization: Solid-state magic-angle spinning (MAS) nuclear magnetic resonance (NMR) spectra were obtained on a Bruker DRX300 MHz NMR spectrometer. ^{29}Si MAS NMR spectrum was measured at 59.60 MHz using a 7 mm rotor spinning at 4 kHz. The 75.4 MHz ^{13}C CP-MAS spectra were obtained using a 7 mm rotor spinning at 4 kHz. The chemical shifts are reported in ppm relative to tetramethylsilane (TMS) for ^{29}Si and relative to adamantane for ^{13}C.

IR Characterization: FTIR-ATR spectra were recorded using a Nicolet Magna FTIR spectrometer with a narrow band MCT detector and a diamond ATR Golden-Gate accessory (Specac Ltd., London). The spectra were obtained from 128 scans with a resolution of 4 cm^{-1}.

X-ray Photoelectron Spectroscopy: The chemical composition of the surface was investigated by X-ray photoelectron spectroscopy, using a PHI 5600-ci spectrometer (Physical Electronics, Eden Prairie, MN). The main XPS chamber was maintained at a base pressure of $< 8.10^{-9}$ Torr. A monochromatic aluminum X-ray source (Al kα = 1486.6 eV) at 250W was used to record survey spectra (1400–0 eV) and high resolution spectra with charge neutralization. The detection angle was set at 45° with respect to the normal of the surface and the analyzed area was 0.016 cm^2 (aperture 5).

^1H Relaxation Analysis and Relaxometric Properties Measurement: 400 µL of Gd labeled nanoparticles suspensions were pipetted into in 6.0 mm NMR tubes. Longitudinal and transversal relaxation times (T_1 and T_2) were measured with a TD-NMR relaxometer (Bruker Minispec 60 mq, 60 MHz, 37 °C). The amount of Gd in each suspension was precisely measured by ICP-MS (Perkin Elmer Elan 6000) after an optimal digestion procedure in HNO_3 and hydrogen peroxide, in order to leach all Gd^{3+} ions from the silica matrix. Relaxation rates ($1/T_1$ and $1/T_2$) were plotted against Gd concentration values, and relaxivities (r_1 and r_2) were calculated from the slope of these curves.

4.5. MSNs Drug Loading and *In Vitro* Drug Release Assays

Drug Loading: MSN-DTPA-PEG nanoparticles with the optimal percentages of grafted PEG-silane and DTPA-silane, were selected for drug loading measurement procedures. For this, daunorubicin (DNR) is used as model of anticancer molecules. To load daunorubicin, MSN-5.7%DTPA(Gd)-3.2%PEG (25 mg) was suspended in a daunorubicin solution (5 mg mL^{-1}, in methanol). The suspension was shaken for 24 h at RT in the dark. Daunorubicin-loaded nanoparticles (DNR@MSN-5.7%DTPA(Gd)-3.2%PEG) were obtained by centrifugation and

washed very carefully three times, then dried under vacuum. DNR loading efficiency was evaluated by TGA and confirmed by UV-Visible spectroscopy.

In Vitro Release Studies: The *in vitro* drug release studies were performed in physiological conditions mimicking in vivo conditions at 37 °C (PBS at pH = 7.4; acetate buffer solution at pH = 5 and pH = 4). In fact, once the particles are entrapped in the endosomes/lysosomes of cells, they are submitted to rather harsh acidic conditions (pH = [3.5–5.5]). For this, acetate buffers are recommended and commonly used as a verification test for the chemical stability, in particular for FDA-approved MRI nanoparticles.[41] PBS was prepared by dissolving one pouch of phosphate-buffered saline (Sigma Aldrich, Canada) in 1 L of deionized water (yielding 0.01 M PBS solution, pH 7.4 at 25 °C, ionic strength = 162.7 mM). Acetate buffer solution (pH = 4 and pH = 5) was prepared by mixing "v" µL of sodium acetate solution (0.1 M) with "v′" µL of acetic acid (0.1 M). For the acetate buffer at pH = 4 (ionic strength = 100 mM), v = 57.5 µL and v′ = 442.5 µL were used. For the acetate buffer at pH = 5 (ionic strength = 100 mM), v = 350 µL and v′ = 150 µL were used. To measure drug release in PBS, DNR@MSN-DTPA(Gd)-PEG (5 mg) were soaked in PBS pH 7.4 (5 mL) in water bath under moderate shaking at 37 ± 1 °C. At time points, particles were centrifuged, then the supernatant (release medium, 1 mL) was removed, and replaced with fresh medium (1 mL). The percentage of daunorubicin released was evaluated by recording the absorbance of the supernatant at 480 nm. For this, a Varian UV-Vis-NIR Cary 500 Scan spectrophotometer in double beam configuration and in an acrylic cuvette with a 1 cm path length was used. Similar experiments were reproduced in acetate buffer.

4.6. Cell Viability Study

Cell viability was determined by the trypan blue (cell membrane functional activity) and the resazurin (mitochondrial function) assays. For this, P388 cells were incubated with nanoparticles (0–100 µg mL^{-1}) in 96-well plates for 24 h and 48 h, respectively. Then, trypan blue dye solution (0.4% in PBS at pH = 7.4) was added to the cell suspensions. Non-viable (stained) and viable cells were counted (Cellometer *Auto* T4 – Nexcelom Bioscience). For the resazurin assay, 7-hydroxy-10-oxidophenoxazin-10-ium-3-one was added to the cell suspensions, and left for viable cells to reduce the non-fluorescent dye resazurin into the fluorescent resorufin (7-hydroxy-3-isophenoxazin-3-one). Then, the reaction of resazurin into resorufin was quantified by fluorescence measurements (excitation, 530 nm; emission, 590 nm) with a 96-well microtiter plate fluorescence reader (Bio-Tek FL600, Winooski, VT, USA). Background fluorescence emitted from the control wells containing the medium and resazurin without cells was subtracted from fluorescence values obtained in the presence of cells and results were then expressed as a percent of the fluorescence of the control cells.

Supporting Information

Supporting Information is available from the Wiley Online Library or from the author.

Acknowledgements

The authors acknowledge the financial support from the National Science and Engineering Research Council (Canada) and the Fonds québécois de la recherche sur la nature et les technologies (FRQNT). Meryem Bouchoucha is grateful to FRQNT for a PhD fellowship. The authors would like to thank Mr Jacques Lacroix for performing cell viability tests and Dr Pascale Chevalier for XPS analysis. Supporting Information is available online from Wiley InterScience or from the authors.

Received: February 14, 2014
Revised: April 3, 2014
Published online: July 28, 2014

[1] a) V. Mamaeva, C. Sahlgren, M. Lindén, *Adv. Drug Delivery Rev.* **2013**, *65*, 689–702; b) Z. X. Li, J. C. Barnes, A. Bosoy, J. F. Stoddart, J. I. Zink, *Chem. Soc. Rev.* **2012**, *41*, 2590–2605; c) A. Popat, S. B. Hartono, F. Stahr, J. Liu, S. Z. Qiao, G. Q. Lu, *Nanoscale* **2011**, *3*, 2801–2818; d) M. Colilla, B. Gonzalez, M. Vallet-Regi, *Biomaterials Sci.* **2013**, *1*, 114–134; e) F. Tang, L. Li, D. Chen, *Adv. Mater.* **2012**, *24*, 1504–1534; f) J. M. Rosenholm, C. Sahlgren, M. Lindén, *Nanoscale* **2010**, *2*, 1870–1883; g) S. B. Wang, *Microporous Mesoporous Mater.* **2009**, *117*, 1–9; h) M. Manzano, M. Colilla, M. Vallet-Regi, *Expert Opin. Drug Delivery* **2009**, *6*, 1383–1400; i) I. I. Slowing, J. L. Vivero-Escoto, C. W. Wu, V. S. Y. Lin, *Adv. Drug Delivery Rev.* **2008**, *60*, 1278–1288; j) M. Vallet-Regi, F. Balas, D. Arcos, *Angew. Chem. Int. Ed.* **2007**, *46*, 7548–7558; k) S. Saha, K. C. F. Leung, T. D. Nguyen, J. F. Stoddart, J. I. Zink, *Adv. Funct. Mater.* **2007**, *17*, 685–693.

[2] S. H. Wu, C. Y. Mou, H. P. Lin, *Chem. Soc. Rev.* **2013**, *42*, 3862–3875.

[3] a) M. Vallet-Regi, A. Ramila, R. P. del Real, J. Perez-Pariente, *Chem. Mater.* **2001**, *13*, 308–311; b) J. Andersson, J. Rosenholm, S. Areva, M. Linden, *Chem. Mater.* **2004**, *16*, 4160–4167; c) Q. L. Tang, Y. Xu, D. Wu, Y. H. Sun, *Chem. Lett.* **2006**, *35*, 474–475; d) A. L. Doadrio, E. M. B. Sousa, J. C. Doadrio, J. P. Pariente, I. Izquierdo-Barba, M. Vallet-Regi, *J. Control Release* **2004**, *97*, 125–132; e) J. C. Doadrio, E. M. B. Sousa, I. Izquierdo-Barba, A. L. Doadrio, J. Perez-Pariente, M. Vallet-Regi, *J. Mater. Chem.* **2006**, *16*, 462–466; f) T. A. Xia, M. Kovochich, M. Liong, H. Meng, S. Kabehie, S. George, J. I. Zink, A. E. Nel, *ACS Nano* **2009**, *3*, 3273–3286; g) Y. Chen, C. Chu, Y. C. Zhou, Y. F. Ru, H. R. Chen, F. Chen, Q. J. He, Y. L. Zhang, L. L. Zhang, J. L. Shi, *Small* **2011**, *7*, 2935–2944; h) X. Li, Q. R. Xie, J. X. Zhang, W. L. Xia, H. C. Gu, *Biomaterials* **2011**, *32*, 9546–9556.

[4] a) X. Li, R. X. Qiam, J. Zhang, W. Xia, H. Gu, *Biomaterials* **2011**, *32*, 9546–9556; b) J. Lu, M. Liong, J. I. Zink, F. Tamanoi, *Small* **2007**, *3*, 1341–1346; c) H. A. Meng, M. Liong, T. A. Xia, Z. X. Li, Z. X. Ji, J. I. Zink, A. E. Nel, *ACS Nano* **2010**, *4*, 4539–4550; d) J. Lu, M. Liong, Z. X. Li, J. I. Zink, F. Tamanoi, *Small* **2010**, *6*, 1794–1805; e) H. A. Meng, M. Xue, T. A. Xia, Y. L. Zhao, F. Tamanoi, J. F. Stoddart, J. I. Zink, A. E. Nel, *J. Am. Chem. Soc.* **2010**, *132*, 12690–12697; f) T. W. Kim, I. I. Slowing, P. W. Chung, V. S. Y. Lin, *ACS Nano* **2011**, *5*, 360–366; g) V. Mamaeva, J. M. Rosenholm, L. T. Bate-Eya, L. Bergman, E. Peuhu, A. Duchanoy, L. E. Fortelius, S. Landor, D. M. Toivola, M. Lindén, C. Sahlgren, *Mol. Ther.* **2011**, *19*, 1538–1546; h) J. M. Hillegass, S. R. Blumen, K. Cheng, M. B. MacPherson, V. Alexeeva, S. A. Lathrop, S. L. Beuschel, J. L. Steinbacher, K. J. Butnor, M. E. Ramos-Nino, A. Shukla, T. A. James, D. J. Weiss, D. J. Taatjes, H. I. Pass, M. Carbone, C. C. Landry, B. T. Mossman, *Int. J. Cancer* **2011**, *129*, 233–244; i) Q. Zhang, F. Liu, K. T. Nguyen, X. Ma, X. J. Wang, B. G. Xing, Y. L. Zhao, *Adv. Funct. Mater.* **2012**, *22*, 5144–5156.

[5] a) K. H. Bae, H. J. Chung, T. G. Park, *Mol. Cells* **2011**, *31*, 295–302; b) H. Meng, M. Xue, T. Xia, Z. X. Ji, D. Y. Tarn, J. I. Zink, A. E. Nel, *ACS Nano* **2011**, *5*, 4131–4144.

[6] P. S. Low, W. A. Henne, D. D. Doorneweerd, *Acc. Chem. Res.* **2008**, *41*, 120–129.

[7] a) J. M. Rosenholm, V. Mamaeva, C. Sahlgren, M. Lindén, *Nanomedicine* **2012**, *7*, 111–120; b) W. X. Mai, H. Meng, *Integrative Biology* **2013**, *1*, 19–28; c) M. Benezra, O. Penate-Medina, P. B. Zanzonico, D. Schaer, H. Ow, A. Burns, E. DeStanchina, V. Longo, E. Herz, S. Iyer, J. Wolchok, S. M. Larson, U. Wiesner, M. S. Bradbury, *J. Clin. Invest.* **2011**, *121*, 2768–2780.

[8] J. E. Lee, N. Lee, T. Kim, J. Kim, T. Hyeon, *Acc. Chem. Res.* **2011**, *44*, 893–902.

[9] D. Yoo, J. H. Lee, T. H. Shin, J. Cheon, *Acc. Chem. Res.* **2011**, *44*, 863–874.

[10] a) R. Weissleder, *Science* **2006**, *312*, 1168–1171; b) G.-P. Yan, L. Robinson, P. Hogg, *Radiography* **2007**, *13*, e5–e19.

[11] a) Q. J. He, J. M. Zhang, J. L. Shi, Z. Y. Zhu, L. X. Zhang, W. B. Bu, L. M. Guo, Y. Chen, *Biomaterials* **2010**, *31*, 1085–1092; b) C. P. Tsai, C. Y. Chen, Y. Hung, F. H. Chang, C. Y. Mou, *J. Mater. Chem.* **2009**, *19*, 5737–5743.

[12] a) Q. J. He, Z. W. Zhang, F. Gao, Y. P. Li, J. L. Shi, *Small* **2011**, *7*, 271–280; b) X. X. He, H. L. Nie, K. M. Wang, W. H. Tan, X. Wu, P. F. Zhang, *Anal. Chem.* **2008**, *80*, 9597–9603; c) K. F. Pirollo, E. H. Chang, *Trends in biotechnology* **2008**, *26*, 552–558; d) F. M. Veronese, G. Pasut, *Drug Discov. Today* **2005**, *10*, 1451–1458.

[13] a) V. Cauda, C. Argyo, T. Bein, *J. Mater. Chem.* **2010**, *20*, 8693–8699; b) M. Prokopowicz, J. Lukasiak, *J. Non-Cryst. Solids* **2010**, *356*, 1711–1720; c) Y. S. Lin, N. Abadeer, C. L. Haynes, *Chem. Commun.* **2011**, *47*, 532–534.

[14] a) J. J. Davis, W. Y. Huang, G. L. Davies, *J. Mater. Chem.* **2012**, *22*, 22848–22850; b) F. Carniato, L. Tei, A. Arrais, L. Marchese, M. Botta, *Chem. Eur. J.* **2013**, *19*, 1421–1428; c) K. M. L. Taylor, J. S. Kim, W. J. Rieter, H. An, W. L. Lin, W. B. Lin, *J. Am. Chem. Soc.* **2008**, *130*, 2154; d) J. L. Vivero-Escoto, K. M. L. Taylor-Pashow, R. C. Huxford, J. Della Rocca, C. Okoruwa, H. Y. An, W. L. Lin, W. B. Lin, *Small* **2011**, *7*, 3519–3528.

[15] Y. Liu, N. Zhang, *Biomaterials* **2012**, *33*, 5363–5375.

[16] F. Carniato, L. Tei, M. Cossi, L. Marchese, M. Botta, *Chem. Eur. J.* **2010**, *16*, 10727–10734.

[17] F. Carniato, L. Tei, W. Dastru, L. Marchese, M. Botta, *Chem. Commun.* **2009**, 1246–1248.

[18] a) N. K. Mal, M. Fujiwara, Y. Tanaka, *Nature* **2003**, *421*, 350–353; b) S. Angelos, N. M. Khashab, Y. W. Yang, A. Trabolsi, H. A. Khatib, J. F. Stoddart, J. I. Zink, *J. Am. Chem. Soc.* **2009**, *131*, 12912; c) Y. L. Zhao, Z. X. Li, S. Kabehie, Y. Y. Botros, J. F. Stoddart, J. I. Zink, *J. Am. Chem. Soc.* **2010**, *132*, 13016–13025; d) H. P. Rim, K. H. Min, H. J. Lee, S. Y. Jeong, S. C. Lee, *Angew. Chem. Int. Ed.* **2011**, *50*, 8853–8857; e) F. Muhammad, M. Guo, W. Qi, F. Sun, A. Wang, Y. Guo, G. Zhu, *J. Am. Chem. Soc.* **2011**, *133*, 8778–8781; f) A. Popat, J. Liu, G. Q. Lu, S. Z. Qiao, *J. Mater. Chem.* **2012**, *22*, 11173–11178; g) R. Guillet-Nicolas, A. Popat, J. L. Bridot, G. Monteith, S. Z. Qiao, F. Kleitz, *Angew. Chem. Int. Ed.* **2013**, *52*, 2318–2322.

[19] a) C. Park, H. Kim, S. Kim, C. Kim, *J. Am. Chem. Soc.* **2009**, *131*, 16614; b) A. Schlossbauer, J. Kecht, T. Bein, *Angew. Chem. Int. Ed.* **2009**, *48*, 3092–3095.

[20] a) R. Liu, X. Zhao, T. Wu, P. Y. Feng, *J. Am. Chem. Soc.* **2008**, *130*, 14418; b) H. Kim, S. Kim, C. Park, H. Lee, H. J. Park, C. Kim, *Adv. Mater.* **2010**, *22*, 4280.

[21] a) C. Park, K. Lee, C. Kim, *Angew. Chem. Int. Ed.* **2009**, *48*, 1275–1278; b) H. Yan, C. Teh, S. Sreejith, L. L. Zhu, A. Kwok, W. Q. Fang, X. Ma, K. T. Nguyen, V. Korzh, Y. L. Zhao, *Angew. Chem. Int. Ed.* **2012**, *51*, 8373–8377.

[22] a) I. F. Tannock, D. Rotin, *Cancer Res.* **1989**, *49*, 4373–4384; b) L. E. Gerweck, K. Seetharaman, *Cancer Res.* **1996**, *56*, 1194–1198.

[23] K. Glunde, S. E. Guggino, M. Solaiyappan, A. P. Pathak, Y. Ichikawa, Z. M. Bhujwalla, *Neoplasia* **2003**, *5*, 533–545.

[24] I. P. Huang, S. P. Sun, S. H. Cheng, C. H. Lee, C. Y. Wu, C. S. Yang, L. W. Lo, Y. K. Lai, *Mol. Cancer Ther.* **2011**, *10*, 761–769.

[25] L. Yuan, Q. Q. Tang, D. Yang, J. Z. Zhang, F. Y. Zhang, J. H. Hu, *J. Phys. Chem. C* **2011**, *115*, 9926–9932.

[26] Y. N. Zhao, J. L. Vivero-Escoto, I. I. Slowing, B. C. Trewyn, V. S. Y. Lin, *Expert Opin. Drug Delivery* **2010**, *7*, 1013–1029.

[27] T. W. Kim, P. W. Chung, V. S. Y. Lin, *Chem. Mater.* **2010**, *22*, 5093–5104.

[28] J. K. Armstrong, r. B. wenby, H. J. Meiselman, T. C. Fisher, *Biophys J.* **2004**, *6*, 4259–4270.

[29] M. C. Goncalves, V. D. Bermudez, R. A. S. Ferreira, L. D. Carlos, D. Ostrovskii, J. Rocha, *Chem. Mater.* **2004**, *16*, 2530–2543.

[30] M. Bouchoucha, M. Jaber, T. Onfroy, J. F. Lambert, B. Y. Xue, *J. Phys. Chem. C* **2011**, *115*, 21813–21825.

[31] M. F. M. Post, in *Stud. Surf. Sci. Catal.*, Vol. *58*, (Eds: E. M. Flanigen, J. C. Jansen, H. V. Bekkum) , Elsevier, **1991**, Ch. 11.

[32] P. Caravan, J. J. Ellison, T. J. McMurry, R. B. Lauffer, *Chem. Rev.* **1999**, *99*, 2293–2352.

[33] a) R. Guillet-Nicolas, J. L. Bridot, Y. Seo, M. A. Fortin, F. Kleitz, *Adv. Funct. Mater.* **2011**, *21*, 4653–4662; b) Y. Z. Shao, L. Z. Liu, S. Q. Song, R. H. Cao, H. Liu, C. Y. Cui, X. Li, M. J. Bie, L. Li, *Contrast Media Mol. Imaging* **2011**, *6*, 110–118; c) J. K. Hsiao, C. P. Tsai, T. H. Chung, Y. Hung, M. Yao, H. M. Liu, C. Y. Mou, C. S. Yang, Y. C. Chen, D. M. Huang, *Small* **2008**, *4*, 1445–1452; d) C. P. Tsai, Y. Hung, Y. H. Chou, D. M. Huang, J. K. Hsiao, C. Chang, Y. C. Chen, C. Y. Mou, *Small* **2008**, *4*, 186–191.

[34] V. A. S. Merbach, É. Tóth, *Angew. Chem.* **2001**, *113*, 4227–4228.

[35] R. Guillet-Nicolas, M. Laprise-Pelletier, M. M. Nair, P. Chevalier, J. Lagueux, Y. Gossuin, L. Laurent, F. Kleitz, M. A. Fortin, *Nanoscale* **2013**, *5*, 11499–11511.

[36] A. Popat, J. Liu, Q. H. Hu, M. Kennedy, B. Peters, G. Q. Lu, S. Z. Qiao, *Nanoscale* **2012**, *4*, 970–975.

[37] J. Siepmann, N. A. Peppas, *Adv. Drug Delivery Rev.* **2001**, *48*, 137–138.

[38] Q. J. He, J. L. Shi, M. Zhu, Y. Chen, F. Chen, *Microporous Mesoporous Mater.* **2010**, *131*, 314–320.

[39] H. Yamada, C. Urata, Y. Aoyama, S. Osada, Y. Yamauchi, K. Kuroda, *Chem. Mater.* **2012**, *24*, 1462–1471.

[40] Z. P. Xu, N. D. Kurniawan, P. F. Bartlett, G. Q. Lu, *Chem, Eur. J.* **2007**, *13*, 2824–2830.

[41] S. Arbab, L. B. Wilson, P. Ashari, E. K. Jordan, B. K. Lewis, J. A. Frank, *NMR Biomed.* **2005**, *18*, 383.